Monthly Notices
of the
ROYAL ASTRONOMICAL SOCIETY

MNRAS **486,** 3636–3646 (2019)
Advance Access publication 2019 April 8

doi:10.1093/mnras/stz958

A fast radio burst with frequency-dependent polarization detected during Breakthrough Listen observations

D. C. Price [1,2] G. Foster [2,3]★ M. Geyer [4] W. van Straten [5] V. Gajjar,[2,6] G. Hellbourg,[2,7] A. Karastergiou,[3,8,9] E. F. Keane [10] A. P. V. Siemion,[2,11,12,13] I. Arcavi,[14,15,16]† R. Bhat,[7] M. Caleb,[17] S.-W. Chang,[18,19,20] S. Croft,[2] D. DeBoer,[2] I. de Pater,[2] J. Drew,[21] J. E. Enriquez,[2,11] W. Farah [1] N. Gizani,[2,22] J. A. Green,[23] H. Isaacson,[2] J. Hickish,[2] A. Jameson,[1,19] M. Lebofsky,[2] D. H. E. MacMahon,[2] A. Möller [18,19] C. A. Onken,[18,19] E. Petroff [24] D. Werthimer,[2,6] C. Wolf [18,19] S. P. Worden[21] and Y. G. Zhang[2]

Affiliations are listed at the end of the paper

Accepted 2019 April 2. Received 2019 March 30; in original form 2019 January 22

ABSTRACT

Here, we report on the detection and verification of fast radio burst FRB 180301, which occurred on UTC 2018 March 1 during the Breakthrough Listen observations with the Parkes telescope. Full-polarization voltage data of the detection were captured – a first for non-repeating FRBs – allowing for coherent de-dispersion and additional verification tests. The coherently de-dispersed dynamic spectrum of FRB 180301 shows complex, polarized frequency structure over a small fractional bandwidth. As FRB 180301 was detected close to the geosynchronous satellite band during a time of known 1–2 GHz satellite transmissions, we consider whether the burst was due to radio interference emitted or reflected from an orbiting object. Based on the pre-ponderance of our verification tests, we cannot conclusively determine FRB 180301 to be either astrophysical or anthropogenic in origin.

Key words: methods: data analysis – methods: observational.

1 INTRODUCTION

Fast radio bursts (FRBs), first reported by Lorimer et al. (2007), are now a routinely detected – but none the less rare – class of transient radio sources of inferred extragalactic origin (e.g. Thornton et al. 2013; Caleb et al. 2017; Ravi 2019), see FRBCAT[1] for an up-to-date catalogue (Petroff et al. 2016). Identifying the sources of FRBs and understanding their emission mechanisms are areas of active research within astronomy. Given their extreme luminosities (isotropic burst energies $>10^{40}$ erg, Dolag et al. 2015) and their inferred cosmological distances, FRBs could be used as cosmological probes (Deng & Zhang 2014; Zhou et al. 2014; Keane 2018; Walters et al. 2018)

To unambiguously prove an extragalactic origin of an FRB, many surveys are focused on using interferometric arrays to localize the source to host galaxies at the time of detection (e.g. Law et al. 2015; Burke-Spolaor et al. 2016; Bannister et al. 2017; Caleb et al. 2017). Further strides towards understanding the nature of FRBs come from more complete sampling of frequency space (Chawla et al. 2017; CHIME/FRB Collaboration 2018, 2019a), and capturing high-time resolution voltage data of a detection (Farah et al. 2018).

To date, only two FRBs have been shown to repeat: FRB 121102 (Spitler et al. 2016) and FRB 180814.J0422 + 73 (CHIME/FRB Collaboration 2019b). The repetition of FRB 121102 allowed interferometric localization and host galaxy identification via follow-up observations (Chatterjee et al. 2017). These observations unambiguously showed FRB 121102 to be astrophysical in origin, at a distance $z \lesssim 0.192$. While FRB 121102 appears to have active and non-active phases, no underlying periodicity has been detected (Zhang et al. 2018). Efforts to localize the recently discovered FRB 180814.J0422 + 73 are ongoing (CHIME/FRB Collaboration 2019b).

Nevertheless, it cannot yet completely be ruled out that some fraction of FRBs are false positives from radio-frequency interference (RFI) as FRB-like RFI is known to exist. A subset of FRB-like signals, dubbed 'perytons', showed signs of near-field terrestrial origin (Burke-Spolaor et al. 2011); eventually, these signals were shown to be caused by an on-site interferer (Petroff et al. 2015b). A

★ E-mail: griffin.foster@gmail.com
† Einstein Fellow
[1] http://frbcat.org/

variety of FRB-like RFI is presented in Foster et al. (2018), along with a verification framework aimed at limiting false positives. (In practice, all one can do is perform as many verification tests as the data allow.) The FRBs reported so far pass all of the tests that it has been possible to perform. However, as we collect increasingly rich information, we can be increasingly rigorous in our verification. This is important as the understanding of the diverse manifestations of RFI is incomplete.

FRBs display varying frequency and polarization characteristics that may be intrinsic or extrinsic to the emission mechanism. Several FRB events – including FRB 110523 (Masui et al. 2015), FRB 170827 (Farah et al. 2018), and FRB 121102 (Gajjar et al. 2018; Michilli et al. 2018) – show spectral modulation on scales of order ∼1 MHz. Shannon et al. (2018) recently reported 20 FRBs detected with the Australian Square-Kilometre Array Telescope Pathfinder (ASKAP), all of which exhibit spectral modulation. Similarly, spectral modulation is also apparent in the 13 bursts detected using the Canadian Hydrogen Intensity Mapping Experiment (CHIME; CHIME/FRB Collaboration 2019a). If intrinsic to the source, the frequency-modulated emission is distinctly different from the broad-band emission associated with possible progenitors such as (young) pulsars and magnetars (Jankowski et al. 2018). In most cases, however, the modulated emission has been attributed to propagation effects, namely inter and intragalactic scintillation.

Polarization properties and Faraday rotation measure (RM) have also been measured for a number of FRBs (Caleb et al. 2018). Large polarization fractions imply the existence of strong magnetic fields in the progenitor or its immediate environment, while large RMs imply strong magnetic fields along the line of sight. A significant linear polarization fraction was reported for FRBs 110523, 150215, 150418, 150807, 151230, and 160102; circular polarization, while less common, is exhibited by FRB 140514, 150215, and 160102 (see table 1 of Caleb et al. 2018 for a summary of polarization properties). Measurements of RMs (inconsistent with zero) are reported for FRBs 110523, 150807, and 160102. FRB 121102 remarkably exhibits an RM in excess of 10^5 rad m^{-2} and appears to evolve with time (Gajjar et al. 2018; Michilli et al. 2018)

As the number of detected FRBs increases, it may become apparent that there are distinct classes, and that the broadly varying burst characteristics are due to different emission mechanisms. Statistically robust relationships between observed quantities may also become apparent. For example, from analysis events detected with Parkes and of 20 FRB events detected with ASKAP, Shannon et al. (2018) report a relationship between dispersion and brightness. A relationship between dispersion and scattering also appears to hold (e.g. CHIME/FRB Collaboration 2019a).

Here, we report the detection of a highly polarized FRB, henceforth FRB 180301. The FRB was detected during Breakthrough Listen (BL) observations of the Galactic plane (Isaacson et al. 2017; Worden et al. 2017). The remainder of this paper is structured as follows. The detection of FRB 180301 is described in Section 2, and its detailed verification in Section 3, following procedures set out in Foster et al. (2018). In particular, we consider evidence for the event being related to a geosynchronous satellite. Details of follow-up observations are given in Section 4. In Section 5, we discuss our findings, with conclusions drawn in Section 6.

2 OBSERVATIONS

FRB 180301 was detected on UTC 2018 March 1 at 07:34:57.969 (MJD 58178.3159487, referenced at 1415 MHz) during BL observations with the CSIRO Parkes 64-m radio telescope (see Appendix for program details). The event occurred in beam 03 of the 21-cm multibeam receiver, the J2000 coordinates of the beam centre during the event were (06:12:43.4, 04:33:44.8), with corresponding Galactic (l, b) coordinates (204.412°, −6.481°); the full width at half-maximum (FWHM) width of the beam is ∼14.1 arcmin. After initial verification, an *Astronomer's Telegram* was issued to allow for immediate follow-up by other facilities (Price et al. 2018b).

FRB 180301 was detected in real-time using the Berkeley–Parkes–Swinburne Recorder (BPSR) and HI-Pulsar system (Keith et al. 2010; Price et al. 2016; Keane et al. 2018), which is configured to run in parallel with the BL digital recorder (Price et al. 2018a). Running BPSR is an addition to the original mode of operation, to allow commensal science during BL observations. BPSR records dynamic spectra with a time resolution of 64 μs, and channel resolution of 390.625 kHz, spanning the receiver's usable band 1.182–1.522 GHz. The BPSR system performs a brute-force incoherent de-dispersion search (Barsdell et al. 2012) in real-time, alerting observers via email to candidate FRB events. The BPSR and BL systems are fully independent, and were both recording data at the time of the event.

The BPSR incoherent search pipeline identified FRB 180301 as a candidate FRB event with a signal-to-noise ratio (S/N) of ∼16 at a dispersion measure (DM) of 520 pc cm^{-3}, using a 2.048 ms boxcar filter; a dynamic spectrum plot of this detection is shown in fig. 10 of Price et al. (2018a). Shortly after visual inspection of the candidate signal, we interrupted regular BL observations, and undertook follow-up observations and calibration procedures.

FRB 180301 was detected in data from both BPSR and the BL recorder; for the analysis presented in this paper, we primarily use BL data products. The BL data recorder system records complex voltage products over 308 MHz of bandwidth (1.2075–1.5155 GHz) to disc in GUPPI raw format (Ford & Ray 2010), for each of the multibeam receiver's 13 beams. The voltages are coarsely channelized into sub-bands of width 3.5 MHz using a critically sampled polyphase filterbank; further instrument details may be found in Price et al. (2018a). The Parkes BL data recorder shares system design with the BL data recorder at the Green Bank telescope (MacMahon et al. 2018), used in the detection of FRB events from FRB 121102 over 4–8 GHz (Gajjar et al. 2018; Zhang et al. 2018).

Nyquist-sampled dual-polarization voltage-level products were recorded for all receiver beams during the detection of FRB 180301. These data can be coherently de-dispersed to remove temporal smearing, increasing the S/N to 20, and allow finer control of the time and frequency resolution of derived dynamic spectrum. A coherently de-dispersed dynamic spectrum, with a time and frequency resolution of 22 μs and 109.375 kHz, is shown in Fig. 1; a summary of the FRB 180301 detection and its derived properties is given in Table 1.

3 ANALYSIS

Here, we detail observed burst characteristics, and apply the tests presented in Foster et al. (2018) as a framework to verify FRB 180301 as astrophysical. A heat map of these test results is shown in Fig. 2, the individual tests are discussed throughout this section. Flux calibration was performed by observing calibrator PKS1934 − 638 in each beam at the beginning of the observation, and polarization calibration was performed with noise diode reference observations. Beam 03 had a frequency-averaged system equivalent flux density (SEFD) of ∼37 Jy. This is higher than the central beam that typically has an SEFD of ∼30 Jy, predominantly due to dish optics (Staveley-Smith et al. 1996). Assuming the pulse

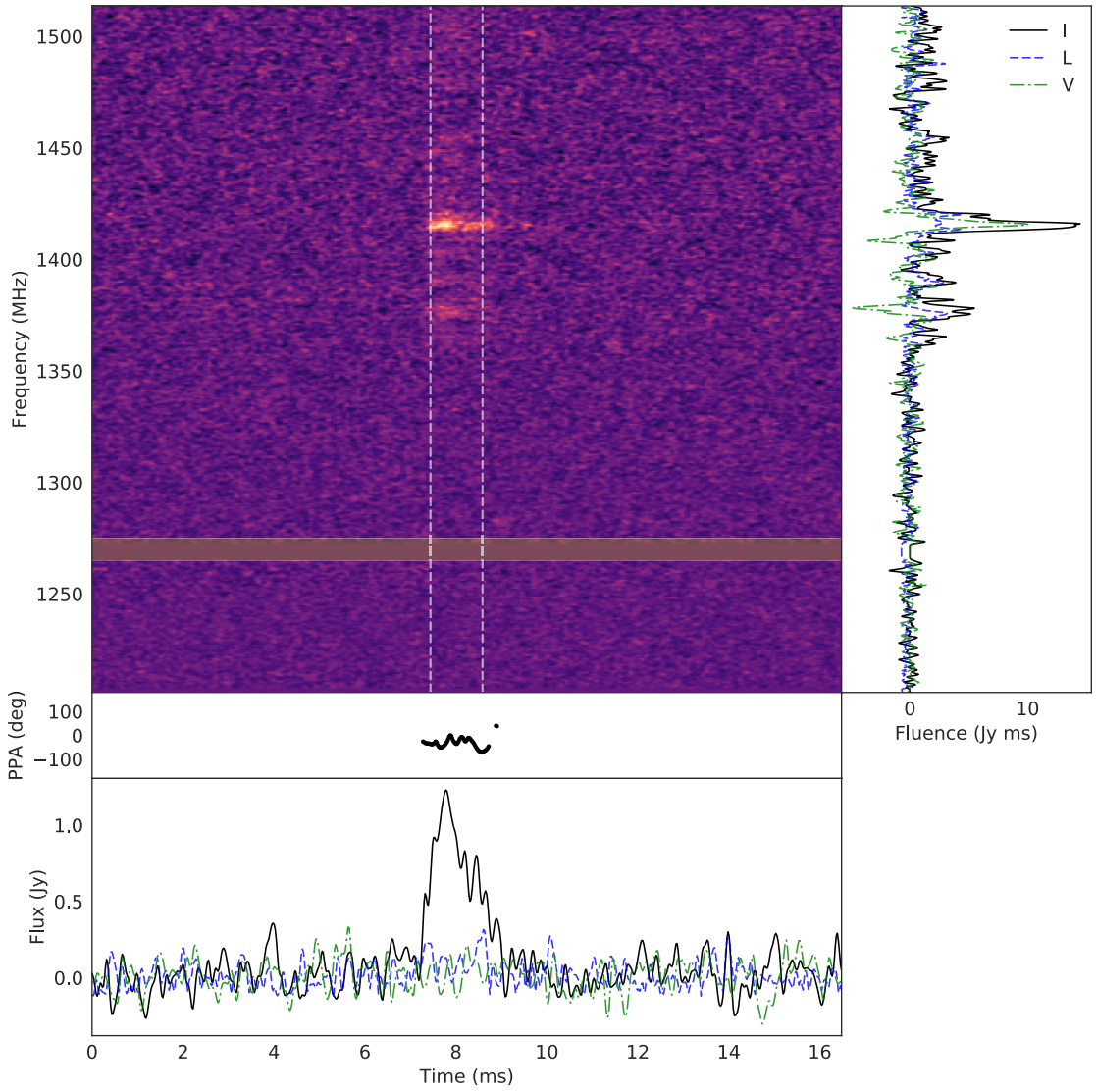

Figure 1. FRB 180301 coherently de-dispersed with a DM of 522 ± 5 pc cm^{-3} to a resolution of 22 μs and 109.375 kHz, with a Gaussian noise filter (88 μs, 220 kHz) applied. No RM correction has been applied. Central figure is the Stokes I dynamic spectrum. Summed spectrum between the white dashed lines is shown on the right; Stokes L and Stokes V are plotted in the blue dashed and green dashed lines, respectively. The summed profile and polarization position angle are plotted in the bottom of the figure. Persistent RFI around ∼1270 MHz has been flagged.

occurred near the centre of beam 03, the frequency-averaged profile has a peak flux of 1.23 Jy. This is more than twice the originally reported peak flux since using coherent de-dispersion has reduced smearing and allowed for the main pulse to be time resolved.

3.1 Radio-frequency interference

To assure the quality of the detection, we investigated the state of the telescope and RFI environment. At the beginning of the observation, calibrator source PKS1934-638 was observed in each beam at the expected S/N. The local time during detection was early evening, meaning that the visitor's centre is closed, and visitor-related RFI sources are fewer. The overall RFI was low during the time of the detection; the Parkes RFI monitor,[2] which operates over 0.4–3.0 GHz, does not show any notable RFI events during the observation period. Persistent RFI associated with Global Navigation Satellite System transmitters around 1207 MHz, 1246 MHz, and 1270 MHz regularly seen in Parkes data were present, and removed during calibration. As flux of the pulse was not seen in the lower half of the band, there is no expectation that this RFI is the progenitor of the observed pulse. Following the suggestions in Foster et al. (2018), a DM-trial search from −2000 to 2000 pc cm^{-3} (ΔDM step size of 10 pc cm^{-3}) during the time of detection revealed no significant RFI events.

As the telescope was pointed in the region of the sky where geosynchronous satellites operate (declinations ±15°; Anderson et al. 2015), we extended the low-altitude pointing test in Foster et al. (2018) to also check for the presence of satellites near the beam (within a few degrees). Though commercial satellites are not known to transmit at the frequency of the detected pulse, we still investigated if the source of the event could be due to a satellite. Using public two-line element set orbital parameters of tracked satellites, we found geosynchronous satellites (NSS-11,

[2]https://www.narrabri.atnf.csiro.au/observing/rfi/monitor/rfi_monitor.html#parkes

Table 1. Summary of FRB 180301 detection and derived properties.

Property	Value
Identifier	FRB 180301
UTC date	2018-03-01
UTC time	07:34:57.969
Local time (AEDT)	18:34:57.969
Modified Julian date	58178.3159487
Telescope / Receiver	Parkes 21-cm multibeam
Observing Band	1.2075–1.5155 GHz
Local Coords (alt, az)	41.4°, 45.6°
Celestial (J2000) (α, δ)	$06^h12^m43.4s$, $04^d33^m45.4^s$
Galactic (l, b)	204.412°, −6.481°
Detection S/N	16
Optimal S/N	20
Peak flux density (Jy)	1.2 ± 0.1
DM (pc cm^{-3})	522 ± 5
DM index	−1.9 ± 0.1
Pulse width (W10) (ms)[a]	2.18 ± 0.06
Pulse width (W10) (ms)[b]	0.74 ± 0.05
$\tau_{\rm scattering}$ (ms)*b*	0.71 ± 0.03
RM (rad m^{-2})[c]	−3163 ± 20

[a]Pulse width fit for a Gaussian component model.
[b]Pulse width and scattering time-scale for a scattered Gaussian component model.
[c]RM assuming polarization characteristics are due to Faraday rotation; see Section 3 for details.

TIANLIAN 1-02) and debris from an Ariane 5 rocket – a European satellite launch vehicle – near the beams at the time of the detection (Fig. 3b). NSS-11 is a Ku-band broadcast satellite[3] (12–18 GHz), and Tianlian 1-02 is a Chinese data relay satellite[4]; neither is known to transmit in the 1–2 GHz band. It is possible the event is related to a government satellite – for example, military satellites are known to use *L*-band frequencies – but a complete record of such satellites is not made available publicly.

One of the bright regions of the FRB 180301 dynamic spectrum overlaps with the global positioning system (GPS) L3 band (1381.05 ± 2.5 MHz), operated by the United States Air Force (USAF). The L3 band is used as part of the nuclear detection system payload present on every GPS satellite. The detection systems are tested quarter-yearly by the USAF.[5] The duty cycle of satellite transmission during these testing times is not reported, but appears to be very low. During the detection of FRB 180301 such tests were occurring throughout the satellite constellation (antenna monitor W8 at the Karl G. Jansky Very Large Array detected use of this band throughout the day[6]). The detection of FRB 180301 occurred at approximately the mid-point of a 30-s period associated with GPS L3 signal transmission (Fig. 4), which is suspiciously coincidental. While the total power in Fig. 4 increases during transmission, the L3 signal remains within its specified band, and is too faint to appear in the Parkes RFI monitor data. GPS satellites are in Medium Earth Orbit and use high-power, wide-beam transmitters. Though a GPS satellite was not near the beams (Fig. 3b), a satellite tens of degrees off from the pointing centre is still sufficiently powerful to be detected in the side lobes of all the beams. We note that this satellite emission could possibly go undetected if the spectra had been normalized and re-quantized or if only a short period of time around the burst was examined. We are not able to determine if this L3 transmission is related to the detected burst, or merely coincident in time.

We attempted to further localize the FRB by cross-correlating the complex voltages from each beam with beam 03 to check for beam side-lobe detections, but no detections were made. Additionally, a low-S/N search of the others beams resulted in a non-detection. The brightest spectral structure has an S/N of ∼40, non-detection of this emission in the neighbouring beams indicates the burst occurred near to the centre of beam 03, or that the intrinsic flux was very large but occurred in an advantageous far side lobe of the beam (Macquart & Ekers 2018). Non-detection in adjacent beams indicates the source is likely in the far-field of the dish ($\gtrsim$39 km). Detection occurred when the telescope was locally positioned at azimuth and altitude (45.6°, 41.4°). This mid-altitude pointing is far from the horizon that the pulse is not likely associated with a fixed-position RFI source in the far-field.

To summarize, the GPS L3 emission was detected in all beams with similar amplitude (Fig. 4), presumably through far-beam side lobes, whereas the FRB was detected only in beam 03, likely near the beam centre. This supports the model that the burst is not directly related to the GPS L3 emission.

3.2 Dispersion measure

The peak S/N DM was fit by performing a coherent de-dispersion at the original detected DM of 520 pc cm^{-3}, then incoherently de-dispersing over a range of ±16 pc cm^{-3} in 0.1 increments (Fig. 5). A 2D Gaussian was fit to this trial DM versus time space to find a peak at 522 ± 5 pc cm^{-3}. The voltage data was then coherently de-dispersed at this DM.

A dispersion relation model ν^{β} was fit to the dispersed pulse resulting in a best-fitting relation of $\beta = -1.9 \pm 0.1$. The error in the DM and the dispersion relation fit range are larger than other FRBs detected at Parkes, due to the band-limited nature of the pulse. As a point of comparison, FRBs 110220 and 110703 follow $\beta = -2.003(6)$ and $\beta = -2.000(6)$, respectively (Thornton et al. 2013); FRB 140504 follows $\beta = -2.000(4)$ (Petroff et al. 2015a).

The line-of-sight Galactic DM contribution is 150 pc cm^{-3} using the NE2001 model (Cordes & Lazio 2002) and 252 pc cm^{-3} using the YWM16 model (Yao, Manchester & Wang 2017). The average of these DM model values results in an excess dispersion of ∼320 pc cm^{-3}. An upper limit on the distance to the host can be determined by assuming the excess dispersion is due to only the intergalactic medium (IGM). We used the FRUITBAT[7] code to evaluate distance using the Inoue (2004) and Zhang (2018) models, with cosmological parameters reported in Planck Collaboration VI (2018); the models predict distances $z \lesssim 0.33$ and $z \lesssim 0.37$, respectively. However, there is a large uncertainty in the IGM dispersion measure contribution. FRB 121102, which appears to be in a dense plasma environment (Michilli et al. 2018), has an estimated host DM contribution of 70−270 pc cm^{-3} and a corresponding distance of $z \sim 0.192$ (Marcote et al. 2017). Assuming the same distance to the host galaxy of FRB 180301 would imply a host DM contribution of ∼140 pc cm^{-3}.

3.3 Pulse profile and scattering models

Modelling the pulse profile (Fig. 1, lower plot) as a Gaussian results in a fit width (at 10 per cent of the peak, W10) of 2.18 ± 0.06 ms. The fluence over the W10 width is 1.3 Jy ms. This simple model results

[3]https://www.ses.com/our-coverage/satellites/355
[4]https://nssdc.gsfc.nasa.gov/nmc/spacecraftOrbit.do?id = 2011-032A
[5]https://science.nrao.edu/facilities/gbt/observer-alerts/gps-l3-1381-05-2-5-mhz-test-times
[6]http://www.vla.nrao.edu/cgi-bin/rfi.cgi
[7]https://github.com/abatten/fruitbat

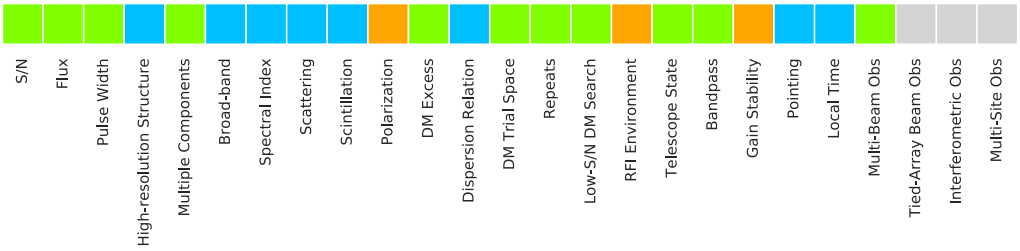

Figure 2. Results heat map of verification tests (Foster et al. 2018) for FRB 180301. Green indicates the test result identical to the prototypical FRB or an ideal observation. Blue indicates the test result similar to the ideal test result, but not identical. Orange indicates the test result significantly different from the ideal result, and could indicate that the FRB is terrestrial. Grey indicates a test that was not valid for the observation.

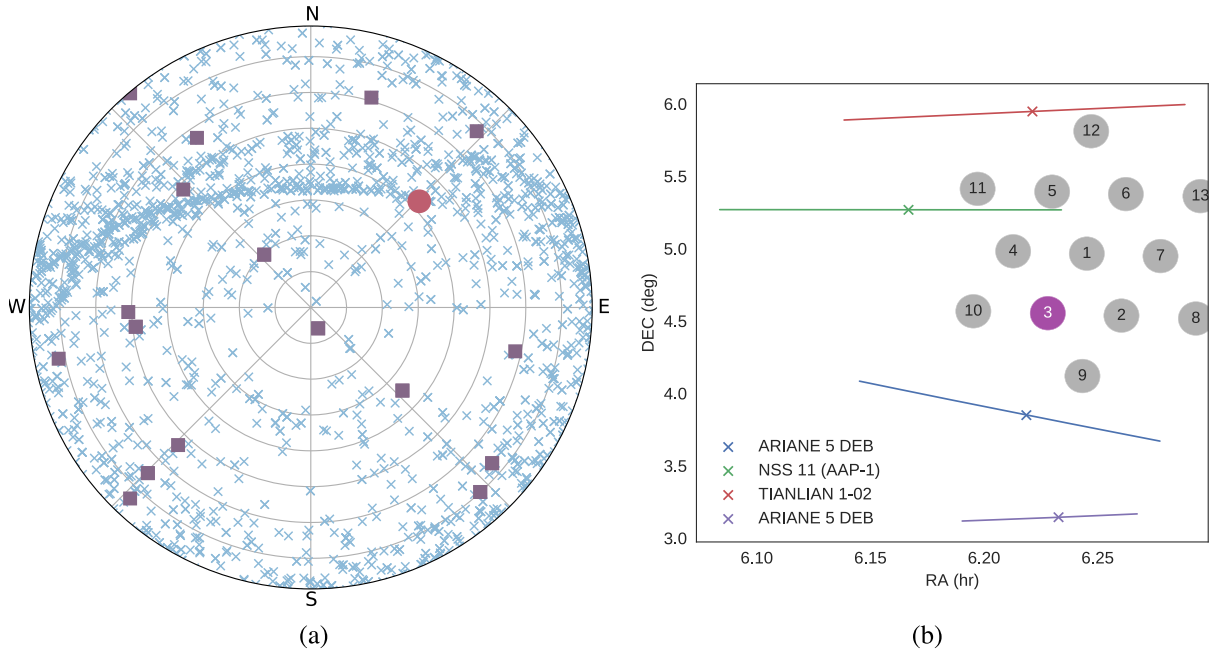

Figure 3. (a) Location of all publicly listed satellites above the horizon for Parkes at UTC 2018-03-01 07:34:19. FRB 180301 is shown as a red circle; GPS satellites are shown as the purple squares. (b) Satellites (NSS-11, TIANLIAN 1-02) and Ariane 5 rocket debris paths near the pointing of the multibeam receivers (circles) within a ±5 min window of the FRB detection in beam 3 (purple). The crosses mark the position of the satellites at time of detection.

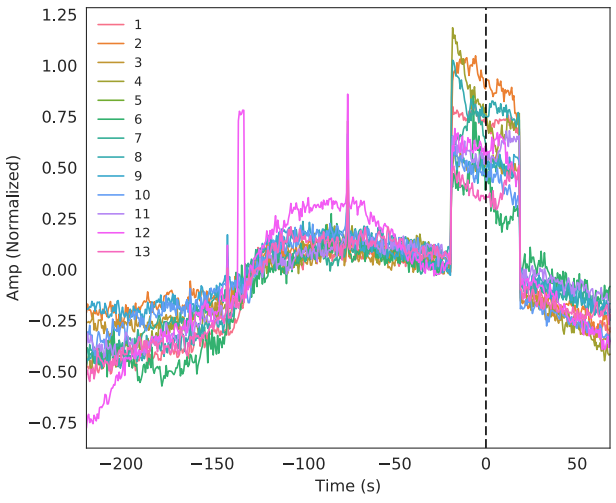

Figure 4. Time series (median removed, normalized) of the total power over the extent of the pulse bandwidth (1350–1460 MHz) in each of the 13 beams. The detection of FRB 180301 (dashed, black) occurred during a period of a GPS L3 test signal transmission.

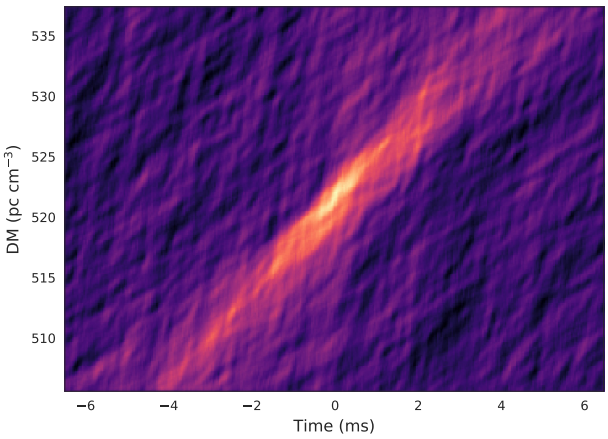

Figure 5. Flux density as a function of DM trial and time. The dynamic spectrum was initially coherently de-dispersed to a DM of 520 pc cm^{-3}, then incoherently de-dispersed $\Delta DM = \pm 16$ pc cm^{-3}.

Table 2. Pulse profile fit for a Gaussian (W10) scattered by an isotropic scattering screen (τ) for the extent of the pulse (1370–1480 MHz) and three sub-regions of the spectrum.

ν (MHz)	W10 (μs)	$\tau_{\rm scatter}$ (μs)
1370–1480	740 ± 50	710 ± 30
1370–1410	770 ± 90	650 ± 50
1410–1420	710 ± 50	800 ± 30
1420–1480	790 ± 130	530 ± 70

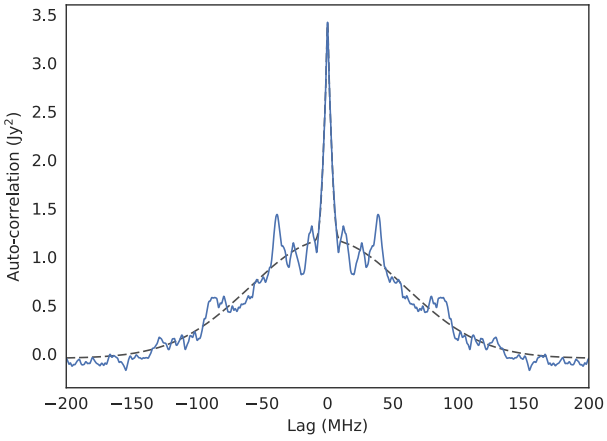

Figure 6. ACF of the time-averaged spectrum. There is a minimum frequency lag scale of ∼6.2 MHz and a maximum of ∼138 MHz, which defines the extent of the spectrum (black dashed).

in a poor fit to the profile, indicating a more complex model, such as a multicomponent or scattered profile model, may be necessary. We find a best-fitting two-component Gaussian with widths 2.41 ± 0.10 and 0.88 ± 0.09 ms separated by 0.41 ms. Alternatively, fitting the (frequency averaged) profile as a Gaussian scattered by an isotropic screen model (Geyer et al. 2017) results in a significantly narrower pulse width (W10) of 0.74 ± 0.05 ms with a scattering time-scale $\tau_{\rm scatter}$ of 0.71 ± 0.03 ms at 1.4 GHz. Comparing the residuals of these two models to normal distributions, by means of a Kolmogorov–Smirnov (KS) test, we conclude that the lower order scattering model performs best (KS test p-values of 0.89 and 0.46, respectively).

We performed the same model fit for three regions (of comparable S/N) within the spectrum: 1370–1410 MHz, across the bright spectral structure around 1415 MHz and at a higher frequency interval of 1420–1480 MHz (see Table 2). We find no evidence of a frequency-dependent scattering time-scale. As there is no clearly preferred pulse profile model, it is possible that FRB 180301 is intrinsically asymmetric.

3.4 Spectro-temporal structure

The pulse spectrum (Fig. 1, right-hand plot) is band-limited with narrow frequency features, potentially due to scintillation. The primary feature of the spectrum is centred around 1415 MHz, this ∼10 MHz wide feature accounts for a third of the total flux. The spectrum shows lower intensity spectral structures between 1350 MHz and the upper edge of the band at 1500 MHz. There is no apparent flux below 1350 MHz. Due to the complex structure of the spectrum, no spectral index model was fit.

Fig. 6 shows the Auto-Correlation Function (ACF) of the time-averaged spectrum over the extent of the W10 pulse width (Fig. 1, right-hand plot). A two Gaussian component model is fit to the ACF. The central peak Full-Width at Half-Maximum (FWHM) is ∼6.2 MHz which is the characteristic frequency scale of the bright structures seen in the spectrum. The band extent of the observed pulse is ∼138 MHz determined by the FWHM of the second model component. The fit scattering time-scale $\tau_{\rm scatter}$ indicates a scintillation bandwidth $\Delta\nu_{\rm d}$ of ≈0.25 kHz (Cordes & Rickett 1998), a much smaller scale compared to the measured characteristic size of the spectral structures. The NE2001 line of sight model (Cordes & Lazio 2002) predicts a scattering time-scale of 2.2 μs and scintillation bandwidth of 50 kHz, two orders of magnitude off from the fit size scales. The spectrum structure could be intrinsic to the source or due to a complex intervening medium, but we are cautious not to over-interpret this result. A single pulse provides insufficient information to build a scintillation model.

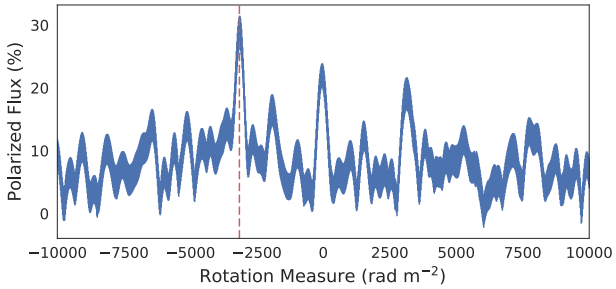

Figure 7. Linear polarization fraction as a function of RM computed during a brute-force RM fit. The peak is at −3163 rad m^{-2}.

3.5 Polarization and rotation measure

The frequency-integrated pulse profile (Fig. 1, bottom plot) shows little to no polarization structure but the spectrum (Fig. 1, right-hand plot) contains features with significant linear and circular polarization.

We attempt to fit a Faraday rotation model to the spectrum to account for the observed linear polarization. We used the RM fitting tool `rmfit` from `PSRCHIVE` (Hotan, van Straten & Manchester 2004) to find the peak linear polarization at an RM of −3163 ± 20 rad m^{-2}. Fig. 7 shows the linear polarization flux as a function of RM. There are significant peaks at 0 rad m^{-2} and +3163 rad m^{-2} indicating Faraday rotation is possibly not a good model to the observed frequency-dependent polarization response.

We explored the Faraday rotation model further by performing a similar QU-fitting analysis as that presented in Michilli et al. (2018). We used a Faraday rotation model $\mathrm{PA}_{\rm Faraday}(\lambda) = \mathrm{PA}_0 + \mathrm{RM}\,\lambda^2$, and the normalized Q and U values were fit for simultaneously. For reference, a lower order model that scales linearly with wavelength, $\mathrm{PA}_{\rm Linear}(\lambda) = \mathrm{PA}_0 + \mathrm{L}\,\lambda$, was also fit. Fig. 8 shows the optimal fit for a Faraday rotated model (green) and a simple λ–relation (magenta). Only regions of the spectrum where the Stokes I exceeds an S/N of 5 were used for the fitting. A brute-force fit of the parameters in both models was performed, resulting in a Faraday rotation model fit of RM = −3156, PA_0 = 0.088, and a linear modal fit of L = −1322, PA_0 = 0.321. Both models result in χ^2 residuals that are within 5 per cent of each other. The residual polarization angle across the band (bottom plot) shows that neither model completely accounts for the observed polarization structure. It is likely the polarization structure is not due to Faraday rotation alone. Satellite communication signals are typically circularly polarized

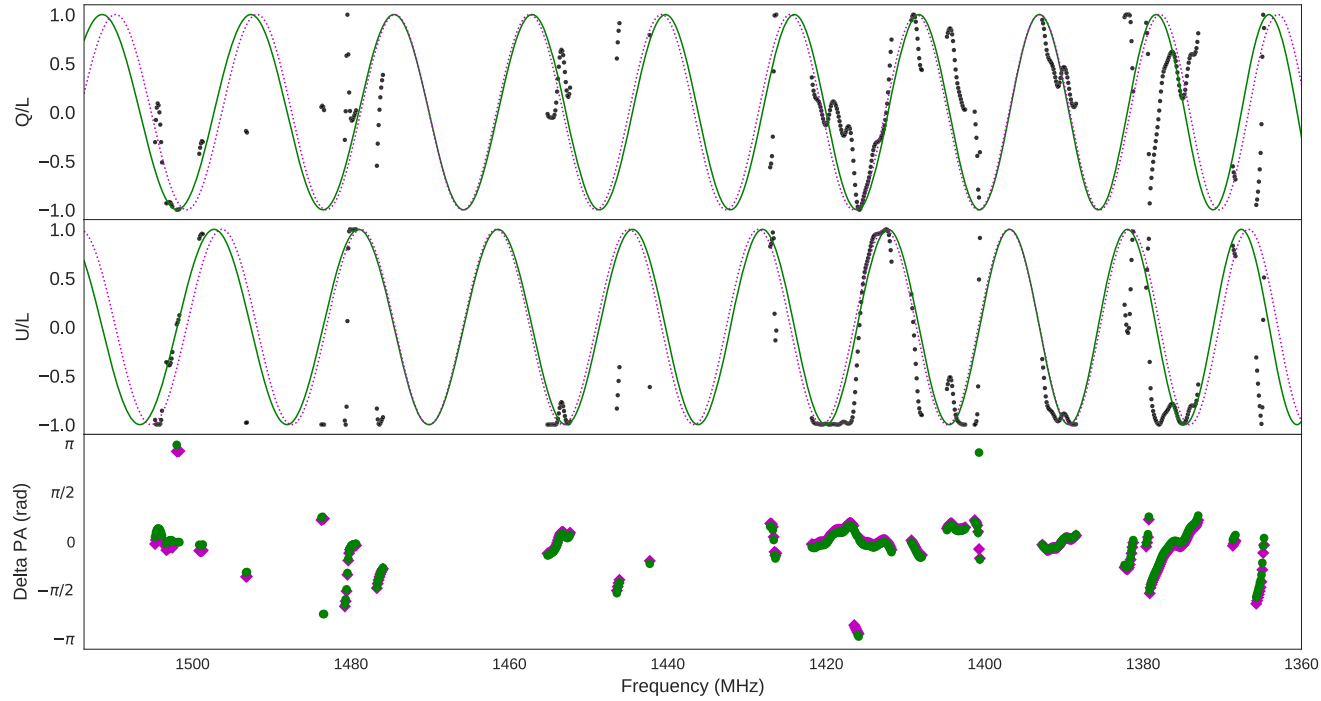

Figure 8. Top and centre plots show best fit from QU-fitting using a λ^2–relation (solid green), and λ–relation (dashed magenta) for channels with an S/N > 5 (the black circles). The bottom plot shows the residual polarization angle for the λ^2–relation model (the green circles) and λ–relation model (the magenta diamonds).

to reduce propagation and antenna alignment effects. If the pulse is anthropogenic, this could explain the polarization structure.

We consider if this frequency-dependent structure is due to a poor polarization calibration. Polarization calibration was performed using a noise diode reference observation, a standard process when observing with Parkes. We found no frequency-dependent polarization excess. This polarization calibration assumes an ideal feed model for a source detected at the beam centre. Since the location of the detection in the beam was unknown, this polarization structure could be due to a frequency-dependent instrumental polarization leakage. Carozzi & Woan (2011) note Parkes has low polarization leakage across a portion of the multibeam band that was measured, but again, this was only reported for the beam centre. If the frequency-dependent polarization structure is instrumental, this would indicate the source was located far from the beam centre. The multibeam receiver far side lobes are not well modelled, as such, we are uncertain if they would induce such a characteristic frequency-dependent structure.

3.6 Cyclostationary analysis

Modulation schemes employed in modern communication exhibit cyclostationary features (Gardner, Napolitano & Paura 2006). To search for evidence of signal modulation that would suggest terrestrial origin – or indeed, emission from a technologically advanced extraterrestrial civilization – we performed cyclic spectroscopy (Antoni 2007, 2009) on the coherently de-dispersed pulse. To maximize S/N, we extracted 10 ms of data around the FRB event from the brightest 3.5 MHz coarse channel (1459.5–1463 MHz). We then computed the cyclic spectral density for the Y-polarization, in which the signal was strongest. No cyclic features were apparent.

To verify this approach, we simulated a transient binary phase-shift keying signal at the apparent S/N of the FRB, and repeated the analysis. No cyclic features were seen, which suggests that the S/N of the FRB is not high enough to preclude communication emissions exhibiting cyclostationary features. At higher S/N (+ 20 dB, i.e. 100x), the cyclic features are indeed apparent.

4 FOLLOW-UP OBSERVATIONS

After post-detection calibration procedures, we observed FRB 180301 for further 82 min to search for repeated bursts. The BPSR real-time detection system did not report any burst candidates during this period. In order to perform a deeper search, we generated Stokes I filterbank files from the BL data with time and frequency resolution of 75 μs and 0.435 MHz. We then searched for pulses over 1207.5–1361.5 MHz and also over 1361.5–1515.5 MHz, with DM range 1–2000 pc cm^{-3} using the HEIMDALL package (Barsdell et al. 2012). We visually inspected dynamic spectra surrounding each candidate event with an S/N > 6 (8661 candidates), but found no significant events similar to FRB 180301.

As reported in Xin, Wang & Wei (2018), we also performed optical follow-up observations of FRB 180301 with the 1.35-m SkyMapper telescope in *g* and *r* band (Keller et al. 2007) using an email-based triggering mechanism. SkyMapper has a wide field of view (5.7deg^2) that fully covers the Parkes localization region of FRB 180301 (∼14 arcmin beam size). This automatic response resulted in a sequence of 10 100-s exposures initiated about 3.2 h after the burst. The first image was obtained at 10:48:28 UTC on 2018 March 1 and the subsequent nine images were slightly dithered to fill in the gaps between Charge-coupled Device (CCDs).

We searched for optical transient candidates within the 14 arcmin Parkes beam using the SkyMapper transient detection pipeline described in Scalzo et al. (2017). A deeper, co-added reference image was taken on 2018 March 9, in order to carry out image subtraction in an optimal manner. Since there is as yet no available

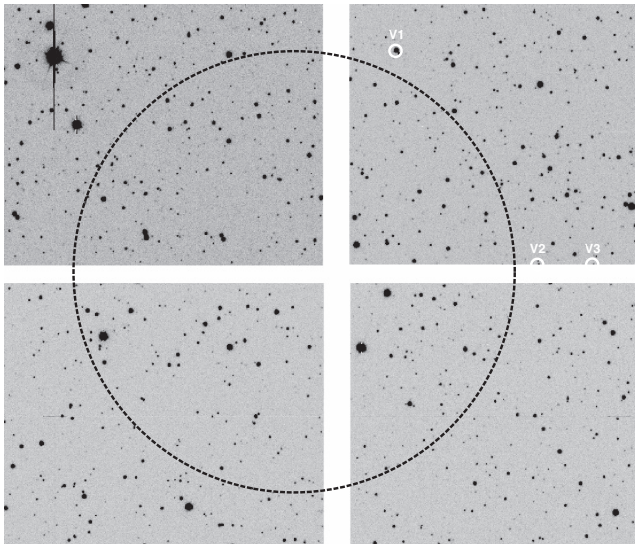

Figure 9. First SkyMapper *r*-band image at the position of FRB 180301. The black circle represents the beam size of the Parkes radio telescope. The white circles indicate three stars detected as variable during the observations, although these are not associated with the FRB.

calibration sources from the first data release of the SkyMapper Southern Survey (Wolf et al. 2018), we use the AAVSO Photometric All Sky Survey catalogue (Henden et al. 2016) to estimate 95 per cent confidence magnitude limits, resulting in point sources detected down to $r \sim 19.4$ and $g \sim 19.2$ mag, which is limited by sky brightness from the moon. We find no transient or variable sources within a 7-arcmin radius of the Parkes beam centre in any of the resultant images (see Fig. 9).

We triggered observations at the position of FRB180301 in the *BVgri* bands with the Las Cumbres Observatory (Brown et al. 2013) 1-m telescope network at 13:22 UTC on 2018 March 1. The first images were obtained at 18:06 UTC on 2018 March 1 with one of the 1-m telescopes at the South African Astronomical Observatory. We find no new sources in the images when performing a visual comparison to archival Digitized Sky Survey images. The images are available for download through the LCO Archive[8] by searching for object 'FRB180301'.

Several follow-up observations of FRB 180301 were reported by other facilities. Anumarlapudi et al. (2018) report no evidence for any hard X-ray transient within the energy range of 20–200 keV. Savchenko et al. (2018σ) report no significant GRB counterpart, estimating a 3σ upper limit on the 75–2000 keV fluence of 4.0×10^{-7} erg cm^2 for a sub-second with a characteristic short GRB spectrum occurring within 300 s of the FRB 180301 detection.

5 DISCUSSION

FRB 180301 does not fit the prototypical model of an FRB, as shown in the verification heat map (Fig. 2). Aside from concerns on the RFI environment, the polarization structure is unusually complex, the pulse appears band limited, we find no preferred pulse profile model, and given the complex spectral structure a spectral index model cannot be fit. Given the ambiguity and atypical features exhibited by FRB 180301, we discuss some concerns, and potential anthropogenic mechanisms, next.

[8]http://archive.lco.global

5.1 Anthropogenic or astrophysical?

The presence of GPS L3 emission during the period of the burst, along with the complex frequency and polarization structure of the pulse, give ambiguous evidence for either an astrophysical or anthropogenic origin.

Also of concern is that three other FRB events, FRB 180309 (Oslowski et al. 2018a), FRB 180311 (Oslowski et al. 2018b), and FRB 180318 (Oslowski, p.c.) were detected with Parkes over the following 17-d period, within ∼140 h of observations (i.e. 0.68 events day^{-1}). This is statistically anomalous. Bhandari et al. (2018) report a total of 19 FRB detections in 306 d of observations with Parkes (0.062 events day^{-1}), and compute an event rate of $1.7^{+1.5}_{-0.9} \times 10^3$ events sky^{-1} day^{-1} above a 2 Jy ms fluence. Based on the Bhandari et al. (2018) event rate for Parkes, we calculate an expectation value of 0.36 events with corresponding Poissonian probability $P(N \geq 4) = 5.4 \times 10^{-4}$ over the ∼140 h of FRB observations during MJD 58178–58196. Nevertheless, while the bunching of events is improbable, one cannot conclusively state that one or more of these bursts is spurious.

An anthropogenic pulse origin does potentially solve some open questions. The band-limited pulse is consistent with an antenna transmission model. The complex polarization structure, which does not appear to follow a Faraday model, could be due to signal modulation. The non-repeating nature is explained as a satellite would be moving and these transmissions are rare. The scattering and scintillation time-scale discrepancy is thus explained as the signal is neither scattered nor scintillating.

Nevertheless, there are several arguments against FRB 180301 being GPS-related RFI. Firstly, the GPS transmission bands are well defined, and do not extend over the band of the detected pulse (although it could be a low-power emission from a malfunctioning or unreported sub-system). Unlike radar systems, GPS satellites are not known to emit chirped pulses that could be mistaken for dispersion. Secondly, the L3 emission was detected in all beams, while FRB 180301 was only detected in a single beam. GPS satellites are ubiquitous, so one might further expect such a signal to have been detected previously, or previous detections have been erroneously reported as FRBs. Finally, the pulse is dispersed, which could be due to a radar system, but no such system is present on GPS satellites.

One possible explanation to FRB 180301's origin is that it is a ground-based L-band (1–2 GHz) wavelength radar reflection used for range-finding during the GPS L3 emission testing. Air Route Surveillance Radar (ARSR) (Niamsuwan, Guner & Johnson 2006; Wang et al. 2012), military radar and telemetry is known to operate at L-band frequencies. GPS was originally a USAF technology developed for military use. A wide-band pulse is common in long-distance range finding; as the observed pulse is band-limited, its duration is consistent with a maximal-power transfer from a ground-based mono-static radar to an object in mid-Earth orbit. Wide-band, dispersed pulses are known to exist and have been previously detected in FRB search pipelines (Foster et al. 2018). The reflected pulse would appear much weaker than the L3 emission, but still dispersed.

Any anthropogenic explanation also needs to explain the frequency-dependent polarization evident in FRB 180301. Polarimetric imaging radar uses polarized pulses to measure the characteristic of surfaces based on scattering, and L-band polarimetric imaging radar systems are known to exist (e.g. Gray et al. 2011).

Katz (2016) argues that space-based radar is unlikely to be the origin of FRBs since the broad range of DMs and pulse

characteristics would suggest an implausible number of space-based radar systems (or systems with a peculiar variety of chirp rates), but does not discuss reflections from ground-based radars. We note that the variety in pulse characteristics could be due to deliberate signal obfuscation. Also, the existence of a population of FRB events with broadly ranging characteristics does not mean that one or more events are spurious, as is the case of the simulated pulses and the events detected by the 25-m Nanshan Telescope reported in (Foster et al. 2018).

Kulkarni et al. (2014) note that the chance reflection of a solar flare off a satellite or the Moon could potentially produce an FRB-like event. Using the solar activity database of Sadykov et al. (2017), we searched for coincident solar flare events; no flares were found, and as such we discount this possibility.

5.2 Instrumental or intrinsic polarization?

Faraday rotation cannot account for the observed circular polarization in the spectrum. Assuming the pulse is astrophysical, the frequency-dependent circular polarization structure indicates either there is significant instrumental polarization leakage, or that the source is intrinsically polarized.

If the source was detected far from the beam centre, it is possible that instrumental polarization leakage is introducing the frequency-dependent structure. However, measurements of the beam response show the first side-lobe level to be below −25 dB (Macquart & Ekers 2018), and as such the intrinsic luminosity of the source would be over two orders of magnitude higher than if located at the beam centre, closer to the luminosities for ASKAP FRBs as reported in Shannon et al. (2018). However, no detection is made in interbeam correlations, meaning that a particularly advantageous (and unlikely) side-lobe response in beam 03 is required. If instrumental polarization leakage is introducing a frequency-dependent structure, then an RM fit is not possible without knowledge of where in the beam the event occurred, and an accurate model for the beam response at that point.

If the source occurred in the primary lobe, then the frequency-dependent polarization structure is likely intrinsic to the source. In this case, the polarization structure may provide information about the underlying emission mechanism of the source. However, as no other FRB reported to date has exhibited similar polarization structure, we caution against overinterpretation. Whatever the origin, an observer should be careful when applying a Faraday rotation model when the location of the detection in the beam is unknown.

5.3 Comparisons with other FRBs

If one concludes that FRB 180301 is astrophysical, and that its polarization structure is primarily due to Faraday rotation, then it bares similarity to FRB 121102 with its complex spectrum and large RM. Though, the fit RM is significantly smaller than that of FRB 121102, no other FRB has a similarly large RM. The magnetic field strength can be estimated to be $\langle B_{\parallel} \rangle = -8\,\mu$G along the line of sight using equation (4) of Han et al. (2006). This is larger than the mean measured large-scale Galactic field strength, but consistent with a high DM source, indicating it is not embedded in a similar environment to FRB 121102 (Michilli et al. 2018).

FRB 180301 has similar spectral characteristics to FRB 170827 (Farah et al. 2018) in that a single, narrow-band component is the dominant contributor to the flux, with lower flux structure spread over a portion of the band. Additionally, there is similar fine structure in the spectrum. None the less, the FRB 180301 profile is wider than FRB 170827, and the events are detected at different frequencies. As only a single polarization was recorded for FRB 170827, its polarization properties are unknown.

FRB 180301, along with FRB 170827 and FRB 121102, are the only events for which complex-voltage data have been captured and reported upon thus far. As other detections used incoherent de-dispersion, and in many cases were discovered in 2-bit data products, it could be the case that most FRBs do indeed have a complex spectrum intrinsic to the source and/or due to scintillation, which is only now becoming apparent with our ability to capture voltage data and perform coherent de-dispersion. Alternatively, it could be that there are multiple observational classes of FRBs: one class that fits the prototypical model without complex frequency structure (Foster et al. 2018), and another class that exhibits complex structure. Repeating sources may also turn out to be a distinct class of event.

Conversely, one might conclude that the polarization structure is a 'smoking gun' that FRB 180301 is anthropogenic. If this were the case, all reported FRBs without complete polarization information (or unambiguous localization) would also be thrown into question. We suggest that until either (a) RFI with similar characteristics to FRB 180301 is identified, or (b) an FRB with unambiguous extragalactic localization is shown to exhibit similar polarization structure to FRB 180301, we should exercise caution that a fraction of reported FRBs may be spurious.

6 CONCLUSIONS

We have reported on the detection of FRB 180301, a highly polarized FRB that exhibits complex frequency structure. Other than FRB 121102, the detection of FRB 180301 is the most complete in terms of addition information for an FRB captured to date. This has allowed a detailed analysis of the coherently de-dispersed pulse and its polarization characteristics.

We performed a rigorous set of tests to verify FRB 180301 as astrophysical, but we are unable to definitively state that FRB 180301 is not related to human activity. Applying coherent de-dispersion to the signal has revealed complex structure, but it is unclear that this structure should be attributed to astrophysical origin. Of particular concern in this instance is the proximity of the event to the geosynchronous orbit belt, and that a GPS testing campaign is known to have been conducted during the day. While circumstantial, the statistically unlikely detection of four FRBs at Parkes within a 17-d period is also troublesome.

Given available data and rigorous tests, it is not always possible to classify the origin of a single-event FRB. FRB 180301 should be taken as a useful example of this. Observations of FRB 121102 have shown, unequivocally, that its emission is astrophysical. The existence of a population of FRBs, detected at multiple telescopes, all displaying astrophysical characteristics, remains strong evidence that FRBs are genuinely an astrophysical phenomena. Nevertheless, as our analysis shows, without precise localization capabilities, conclusive verification of a single event remains challenging. Every FRB reported should be taken cautiously, as they will affect future models and studies.

Interferometric and multisite detection are essential to rule out satellites as FRB progenitors. Arrays with Fresnel zones farther out than Geosynchronous Orbit (GEO) orbits (36 000 km) – which at 1.4 GHz corresponds to 2 km baselines – will be capable of precluding satellites, or chance reflections off space debris, as sources of FRB-like RFI. ASKAP, MeerKAT, and other upcoming instruments meet this criterion.

The complex voltage data and intermediate data products are publicly hosted at the BL data center. Jupyter notebooks with our analysis are hosted on our public git repository.[9]

ACKNOWLEDGEMENTS

We thank Jim Cordes, Jason Hessels, Simon Johnston, Dan Mertely, and Allison Rung for their comments and help. BL is managed by the Breakthrough Initiatives, sponsored by the Breakthrough Prize Foundation. The Parkes radio telescope is part of the Australia Telescope National Facility, which is funded by the Australian Government for operation as a National Facility managed by CSIRO. SkyMapper is owned and operated by the Australian National University's Research School of Astronomy and Astrophysics; the national facility capability is funded through Australian Research Council LIEF grant LE130100104. Parts of this project were conducted by the Australian Research Council Centre of Excellence for All-sky Astrophysics (CAASTRO), through project number CE110001020 and was funded by the Australian Research Council Centre of Excellence for Gravitational Wave Discovery (OzGrav), CE170100004. Support for IA was provided by NASA through the Einstein Fellowship Program, grant PF6-170148.

REFERENCES

Anderson P. V., McKnight D. S., Pentino F., Schaub H., 2015, in Proceedings of a meeting held 12-16 October 2015, Jerusalem, Israel. 66th International Astronautical Congress 2015 (IAC 2015): Space - The Gateway for Mankind's Future. International Astronautical Federation, p. 7
Antoni J., 2007, Mech. Syst. Signal Process., 21, 597
Antoni J., 2009, Mech. Syst. Signal Process., 23, 987
Anumarlapudi A., Aarthy E., Arvind B., Bhalerao V., Bhattacharya D., Rao A. R., Vadawale S., 2018, Astron. Telegram, 11417, 1
Bannister K. W. et al., 2017, ApJ, 841, L12
Barsdell B. R., Bailes M., Barnes D. G., Fluke C. J., 2012, MNRAS, 422, 379
Bhandari S. et al., 2018, MNRAS, 475, 1427
Brown T. M. et al., 2013, PASP, 125, 1031
Burke-Spolaor S., Bailes M., Ekers R., Macquart J.-P., Crawford F., III, 2011, ApJ, 727, 18
Burke-Spolaor S. et al., 2016, ApJ, 826, 223
Caleb M. et al., 2017, MNRAS, 468, 3746
Caleb M. et al., 2018, MNRAS, 478, 2046
Carozzi T. D., Woan G., 2011, IEEE Trans. Antennas Propag., 59, 2058
Chatterjee S. et al., 2017, Nature, 541, 58
Chawla P. et al., 2017, ApJ, 844, 140
CHIME/FRB Collaboration, 2018, ApJ, 863, 48
CHIME/FRB Collaboration, 2019a, Nature, 566, 230
CHIME/FRB Collaboration, 2019b, Nature, 566, 235
Cordes J. M., Lazio T. J. W., 2002, preprint (astro–ph/0207156)
Cordes J. M., Rickett B. J., 1998, ApJ, 507, 846
Deng W., Zhang B., 2014, ApJ, 783, L35
Dolag K., Gaensler B. M., Beck A. M., Beck M. C., 2015, MNRAS, 451, 4277
Enriquez J. E. et al., 2017, ApJ, 849, 104
Farah W. et al., 2018, MNRAS, 478, 1209
Ford J., Ray J., 2010, Fourth International Workshop on High-Performance Reconfigurable Computing Technology and Applications. National Center for Supercomputing Applications, University of Illinois at Urbana-Champaign, p. 1
Foster G. et al., 2018, MNRAS, 481, 2612
Gajjar V. et al., 2018, ApJ, 863, 2
Gardner W. A., Napolitano A., Paura L., 2006, Signal Process., 86, 639
Geyer M. et al., 2017, MNRAS, 470, 2659
Gray D. et al., 2011, in Synthetic Aperture Radar (APSAR), 2011 3rd International Asia-Pacific Conference on [proceedings]. IEEE, Piscataway, N.J, p. 1
Han J. L., Manchester R. N., Lyne A. G., Qiao G. J., van Straten W., 2006, ApJ, 642, 868
Henden A. A., Templeton M., Terrell D., Smith T. C., Levine S., Welch D., 2016, VizieR Online Data Catalog, 2336
Hotan A. W., van Straten W., Manchester R. N., 2004, PASA, 21, 302
Inoue S., 2004, MNRAS, 348, 999
Isaacson H. et al., 2017, Publ. Astron. Soc. Aust., 129, 054501
Jankowski F., van Straten W., Keane E. F., Bailes M., Barr E. D., Johnston S., Kerr M., 2018, MNRAS, 473, 4436
Katz J. I., 2016, ApJ, 818, 19
Keane E. F., 2018, Nat. Astron., 2, 865
Keane E. F. et al., 2018, MNRAS, 473, 116
Keith M. J. et al., 2010, MNRAS, 409, 619
Keller S. C. et al., 2007, Publ. Astron. Soc. Aust., 24, 1
Kulkarni S. R., Ofek E. O., Neill J. D., Zheng Z., Juric M., 2014, ApJ, 797, 70
Law C. J. et al., 2015, ApJ, 807, 16
Lorimer D. R., Bailes M., McLaughlin M. A., Narkevic D. J., Crawford F., 2007, Science, 318, 777
MacMahon D. H. E. et al., 2018, PASP, 130, 044502
Macquart J.-P., Ekers R. D., 2018, MNRAS, 474, 1900
Marcote B. et al., 2017, ApJ, 834, L8
Masui K. et al., 2015, Nature, 528, 523
Michilli D. et al., 2018, Nature, 553, 182
Niamsuwan N., Guner B., Johnson J., 2006, in 2006 IEEE International Symposium on Geoscience and Remote Sensing. IEEE, Denver, CO, USA, p. 2285
Oslowski S. et al., 2018a, Astron. Telegram, 11385, 1
Oslowski S. et al., 2018b, Astron. Telegram, 11396, 1
Petroff E. et al., 2015a, MNRAS, 447, 246
Petroff E. et al., 2015b, MNRAS, 451, 3933
Petroff E. et al., 2016, Publ. Astron. Soc. Aust., 33, e045
Planck Collaboration VI, 2018, A&A, preprint (arXiv:1807.06209)
Price D. C. et al., 2018a, Publ. Astron. Soc. Aust., 35
Price D. C. et al., 2018b, Astron. Telegram, 11376, 1
Price D. C., Staveley-Smith L., Bailes M., Carretti E., Jameson A., Jones M. E., van Straten W., Schediwy S. W., 2016, J. Astron. Instrum., 5, 1641007
Ravi V., 2019, MNRAS, 482, 1966
Sadykov V. M., Kosovichev A. G., Oria V., Nita G. M., 2017, ApJS, 231, 6
Savchenko V. et al., 2018, Astron. Telegram, 11386, 1
Scalzo R. A. et al., 2017, Publ. Astron. Soc. Aust., 34, e030
Shannon R. M. et al., 2018, Nature, 562, 386
Siemion A. et al., 2015, in Advancing Astrophysics with the Square Kilometre Array (AASKA14). p. 116
Spitler L. G. et al., 2016, Nature, 531, 202
Staveley-Smith L. et al., 1996, Publ. Astron. Soc. Aust., 13, 243
Thornton D. et al., 2013, Science, 341, 53
Walters A., Weltman A., Gaensler B. M., Ma Y.-Z., Witzemann A., 2018, ApJ, 856, 65
Wang J., Brookner E., Cornwell P., Gerecke M., Farr J., 2012, IEEE Trans. Aerosp. Electron. Syst., 48, 103
Wolf C. et al., 2018, Publ. Astron. Soc. Aust., 35, e010
Worden S. P. et al., 2017, Acta Astronaut., 139, 98
Xin L., Wang J., Wei J., 2018, Astron. Telegram, 11438, 1
Yao J. M., Manchester R. N., Wang N., 2017, ApJ, 835, 29
Zhang B., 2018, ApJ, 867, L21
Zhang Y. G., Gajjar V., Foster G., Siemion A., Cordes J., Law C., Wang Y., 2018, ApJ, 866, 149
Zhou B., Li X., Wang T., Fan Y.-Z., Wei D.-M., 2014, Phys. Rev. D, 89, 107303

[9] https://github.com/griffinfoster/frb180301-analysis

APPENDIX: BREAKTHROUGH LISTEN

BL is a 10-yr initiative directed at detecting technosignatures that would indicate the presence of advanced life beyond the Earth (Worden et al. 2017). The initial BL program uses the 100-m Robert C. Byrd Green Bank telescope in West Virginia, USA, and the 64-m CSIRO Parkes radio telescope to observe a selection of 1709 nearby stars and 100 nearby galaxies, along with surveying the Galactic plane (Isaacson et al. 2017; Enriquez et al. 2017). In addition, the 2.4-m Automated Planet Finder optical telescope is also being used, to conduct a search for narrow-band optical transmissions from targets within the 1709-star sample. Combined, the observations from these telescopes constitute the most comprehensive search for technosignatures to date.

In the initial years of the program, 25 per cent of the total observing time of the Parkes telescope is assigned for BL activities. Observations are typically scheduled for 10–11 h per day, up to 4–5 times per week. A major component of the BL program at Parkes is a 21-cm wavelength Galactic plane survey, which utilizes the Parkes multibeam receiver (Staveley-Smith et al. 1996). The survey covers Galactic latitudes $|b| < 6.5^\circ$ over the range of Galactic longitudes accessible with Parkes, $-174^\circ < l < 60^\circ$. Similar to the High-Time Resolution Universe (HTRU) survey (Keith et al. 2010), a step-and-stare approach with 5-min pointings is employed. Each beam of the multibeam receiver is separated by 14 arcmin in one plane, and $\sqrt{3} \times 14$ arcmin in the other plane. As the FWHM beamwidth of the receiver is ∼14 arcmin at 21-cm wavelength, interleaved pointings allow for the survey area to be efficiently covered with tessellated pointings (see fig. 2 of Keith et al. 2010).

While the BL survey follows a similar observational strategy to the HTRU and SUrvey for Pulsars and Extragalactic Radio Bursts (SUPERB) surveys (Keane et al. 2018), technosignature searches require a far higher spectral resolution (∼1 Hz; Siemion et al. 2015) than that available in archival data products from the HTRU/SUPERB surveys (∼390 kHz). As such, new digital recorder systems have been installed at both the Parkes and Green Bank observatories to allow voltage capture to disc across the full bandwidth of the available receivers (MacMahon et al. 2018; Price et al. 2018a).

[1]*Centre for Astrophysics & Supercomputing, Swinburne University of Technology, Hawthorn, VIC 3122, Australia*
[2]*Department of Astronomy, University of California Berkeley, Berkeley, CA 94720, USA*
[3]*Astronomy Department, University of Oxford, Keble Rd, Oxford OX13RH, UK*
[4]*SARAO, 2 Fir Street, Black River Park, Observatory, Cape Town 7925, South Africa*
[5]*Institute for Radio Astronomy and Space Research, Auckland University of Technology, PB 92006, Auckland 1142, New Zealand*
[6]*Space Sciences Laboratory, University of California, Berkeley, Berkeley, CA 94720, USA*
[7]*International Centre for Radio Astronomy Research, Curtin University, Bentley, WA 6102, Australia*
[8]*Physics Department, University of the Western Cape, Cape Town 7535, South Africa*
[9]*Department of Physics and Electronics, Rhodes University, PO Box 94, Grahamstown 6140, South Africa*
[10]*SKA Organisation, Jodrell Bank Observatory, Macclesfield, Cheshire SK11 9DL, UK*
[11]*Department of Astrophysics/IMAPP, Radboud University, Nijmegen, 6500, The Netherlands*
[12]*SETI Institute, Mountain View, California, 94043, USA*
[13]*University of Malta, Institute of Space Sciences and Astronomy, Msida MSD 2080, Malta*
[14]*Department of Physics, University of California, Santa Barbara, CA 93106-9530, USA*
[15]*Las Cumbres Observatory, 6740 Cortona Dr Ste 102, Goleta, CA 93117-5575, USA*
[16]*The Raymond and Beverly Sackler School of Physics and Astronomy, Tel Aviv University, Tel Aviv 69978, Israel*
[17]*Jodrell Bank Centre for Astrophysics, the University of Manchester, Manchester, SK11 9DL, UK*
[18]*Research School of Astronomy and Astrophysics, The Australian National University, Canberra, ACT 2611, Australia*
[19]*ARC Centre of Excellence for All-sky Astrophysics (CAASTRO), School of Physics, The University of Sydney, Sydney, NSW 2006, Australia*
[20]*ARC Centre of Excellence for Gravitational Wave Discovery (OzGrav), Swinburne University of Technology, Hawthorne VIC 3122, Australia*
[21]*The Breakthrough Initiatives, NASA Research Park, Bld. 18, Moffett Field, CA, 94035, USA*
[22]*School of Science and Technology, Hellenic Open University, Parodos Aristotelous 18, Patra 263 35, Greece*
[23]*Australia Telescope National Facility, CSIRO, PO Box 76, Epping, NSW 1710, Australia*
[24]*Anton Pannekoek Institute for Astronomy, University of Amsterdam, Science Park 904, NL-1098 XH Amsterdam, The Netherlands*

This paper has been typeset from a TEX/LATEX file prepared by the author.